Turbine Stator Well Geometry Benefits – Method Validation and Design Optimisation

Julien Pohl* and Harvey M. Thompson†
School of Mechanical Engineering, University of Leeds, Leeds, LS2 7JT, UK
Vincenzo Fico‡ and Gary A. Clayton‡
Thermo-Fluids Systems, Rolls-Royce plc., Derby, DE24 8BJ, UK

This paper summarises the two part work carried out during project 7 of work package 3 of the EU funded research project AMEDEO. At first, the outcome of a practical application and extension of a numerical coupled FEA-CFD methodology is presented. Extensive use is made of FEA (solids) and CFD (fluid) modelling techniques to understand the thermo-mechanical behaviour of a turbine stator well cavity, due to the interaction of cooling air supply with the main annulus. In this investigation, two different geometries (baseline and a deflector plate design) with a specific amount of cooling air are modelled and the impact of the structural deflections on the heat transfer is investigated.

The second part focuses on a CFD-based automated optimisation of a turbine stator well (TSW) geometry with an included stationary deflector plate. Experiments as well as numerical simulations have shown that due to the deflector plate the cooling flow is fed more directly into the disc boundary layer, allowing more effective use of less cooling air, leading to improved engine efficiency. Therefore, the deflector plate geometry is embedded in an automated optimisation loop to further reduce the amount of cooling air. The optimisation strategy concentrates on a flexible design parameterisation of the cavity geometry with deflector plate and its implementation in an automatic 3D meshing system. The parameterised geometry is optimised using a metamodel-assisted approach based on regressing Kriging in order to identify the optimum position and orientation of the deflector plate inside the cavity.

Nomenclature

f	Objective function, [-]
g	Constraint, [-]
$\dot{m}_{cool}$	Cooling mass flow rate, [kg/s]
n	Number of design variables, [-]
r	Radius, [m]
Re_ϕ	Rotational Reynolds number, [-]
T_m	Metal temperature, [K]
v_θ	Tangential velocity, [m/s]
y^+	Normalised near wall spacing, [-]
$\mathbf{x}$	Design vector, [-]
β	Swirl fraction, [-]
ω	Rotational speed, [rad/s]
θ_m	Non-dimensional metal temperature, [-]

I. Introduction

Engine components are commonly exposed to air temperatures exceeding the thermal material limit in order to increase the overall engine performance and to maximise the engine specific fuel consumption.

*Marie Curie Fellow and PhD candidate.
†Professor in Computational Fluid Dynamics and academic supervisor.
‡Project partners and specialists in CFD and thermal analyses of secondary air systems.

To prevent the overheating of the materials and thus the reduction of the component life, an internal flow system must be designed to cool the critical engine parts and to protect them. As the coolant flow is bled from the compressor and not used for the combustion an important goal is to minimise the amount of coolant in order to optimise the overall engine performance.

During a typical flight cycle an aero-engine undergoes different operating conditions which cause varying temperatures, pressures, stresses and displacements to the engine components. From an engineering perspective, it is desirable to be able to accurately predict these behaviours in order to stay within the environmental and safety margins and to maximise component life. This also avoids costly experimental engine tests and increases the competitiveness of the aero-engine company in their market.

Predicting the metal temperatures is of paramount importance as they are a major factor in determining the component stresses and lives. In addition, as modern engines operate in ever harsher conditions due to efficiency requirements, the ability to predict thermal displacements becomes very relevant: on one hand, to prevent damage of components due to excessive rubbing, on the other hand, to understand how much air is flowing internally within the secondary air system for cooling and sealing purposes, not only in the design condition but throughout the engine life-span. In order to achieve this aero-engine manufacturers aim to use more and more accurate numerical techniques requiring multi-physics models, including thermo-mechanical finite elements and CFD models, which can be coupled in order to investigate small variations in temperatures and displacements.

This paper summarises the work carried out during project 7 of work package 3 of the EU funded research project AMEDEO (Aerospace Multidisciplinary Enabling DEsign Optimisation)[1] and shows a practical application and extension of the methodology developed during the five year research programme MAGPI (Main Annulus Gas Path Interaction).[2] Extensive use is made of FEA (solids) and CFD (fluid) modelling techniques to understand the thermo-mechanical behaviour of a turbine stator well cavity, due to the interaction of cooling air supply with the main annulus. Previous work based on the same rig showed difficulties in matching predictions to thermocouple measurements near the rim seal gap.[3–6] In this paper, additional results from two previous studies[7,8] are presented, where further use has been made of existing measurements of hot running seal clearances in the MAGPI rig. The structural deflections have been applied to two existing models in order to evaluate the impact in flow interactions and heat transfer in the TSW.

In addition to a baseline test case, a geometry with a stationary deflector plate is modelled and validated for one particular flow case. Experiments as well as numerical simulations have shown that due to the deflector plate the cooling flow is fed more directly into the disc boundary layer, allowing more effective use of less cooling air, leading to improved engine efficiency. Therefore, the deflector plate geometry is embedded in a CFD-based automated optimisation loop to further reduce the amount of cooling air. Full details of this process are summarised in the papers of Pohl et al.[9,10] This work focuses on presenting further results of the same study.

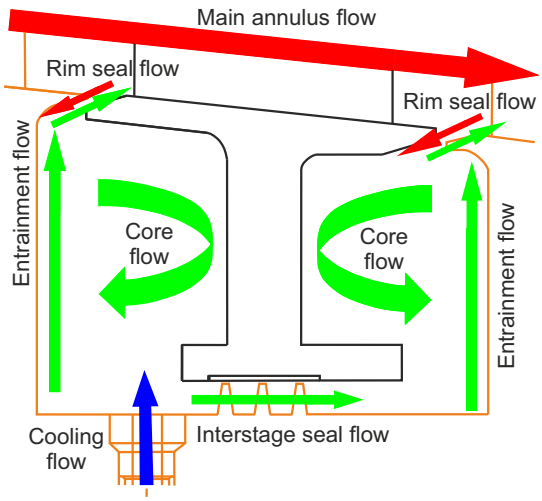

Figure 1. Typical TSW flow structure for the 'baseline geometry'

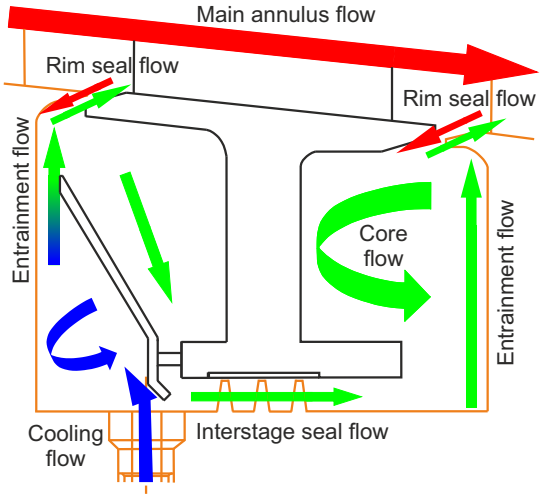

Figure 2. Typical TSW flow structure for the 'deflector geometry'

II. TSW Flow Theory

This section gives an overview of typical flow patterns in two different TSW designs. In Fig. 1, the flow field as it is present in the so called baseline design is shown.[7] Figure 2 depicts the typical flow scenario in a TSW with an integrated stationary deflector plate,[9] which is beneficial with respect to the upstream rotor disc cooling compared to a baseline geometry without a deflector plate. The orange and black geometry contour lines represent rotating and stationary parts, respectively.

For both cases, cooling air is introduced into the upstream cavity radially through a drive arm hole. Other than for the baseline geometry, where a traditional rotor-stator flow is formed,[11] the cooling air does not penetrate the cavity forming a core flow, but instead impinges the deflector plate and is turned towards the rotor disc, by forming a complex 3D vortex flow structure. The cooling air which reaches the upstream rotor disc is then entrained radially outwards by the rotating part of the turbine. The rim seal flow characterises the mixing zone between the hot gas coming from the main annulus and the cooling air. The interaction of these two flows strongly affects the temperatures inside the cavity. Three different flow scenarios in the two TSW designs can be distinguished depending on the amount of cooling air and the size of the interstage seal clearance:[12,13]

Net gas ingestion: If the amount of cooling air is small and/or the interstage seal clearance is large, the rim seal flow is dominated by hot gas entering the cavity.

Net gas egress: If the amount of cooling air is large and/or the interstage seal clearance is tight, the rim seal flow is dominated by cooling air leaving the cavity in the main annulus.

Local ingestion/egress: If the cavity flow is balanced locally hot gas enters the cavity but also cool air enters the main annulus. This phenomenon is driven by the rotor-stator interaction in the main gas path and the turbulent mixing in the rim region.

For both designs, the portion of air/gas mixture staying in the cavity then finds its way to the interstage seal clearance. In the deflector plate design this is guaranteed since the deflector plate is mounted to the stator foot by a few pins, spacers or bolts in order to allow air to pass between these parts, such that the air flow is driven by the presence of a pressure gradient from outer to inner radii between the stator wall and the deflector plate.

Interstage seals are used to reduce the flow of air from the upstream to the downstream stator well cavities. This seal flow is, as mentioned above, largely influenced by the clearance size and also the pressure drop across the seal, which is a function of the upstream and downstream conditions including the pressure drop over the stage in the main annulus. The flow structure in the downstream cavity can then again be described as a traditional rotor-stator flow, consisting of a disc entrainment flow, a core flow and a rim seal exchange flow.[11]

III. Numerical Modeling and Methodology

This section gives a brief overview of the numerical modeling approach and the numerical methods used for the aerothermal coupling and the automated optimisation. At first details are given for the aerothermal coupling approach, which is used to predict the metal temperatures taking into account of the structural deflections. Then, in the second part, the numerical modeling and the parameterisation for the meta-model assisted optimisation process are briefly presented. For full details reference is made to the publications of Pohl et al.[7–10]

III.A. Aerothermal Coupling

The analysis models are based on the MAGPI two-stage turbine test rig.[14,15] Since the turbine was designed to suit the subsequent FEA and CFD analyses, with 39 nozzle guide vanes and 78 rotor blades for each stage, the analysis models could be set-up as sector models at 1/39 th of the complete rotor-stator system keeping the accuracy and the computational costs within feasible limits.

The 3D FEA models, shown in Fig. 3 in grey, are 1/39 th sectors containing the rotor blade rows and discs, the second stage stator vane and the discs, connecting drive arm and stator foot. The deflector geometry additionally contains the sector of the deflector and one scaled bolt.[7] The models are set up to run thermally only. The boundary conditions in the regions of the TSW as well as in the rotor 1 blades and stator 2 vane are coupled to the CFD models. The remaining non-coupled boundary conditions are obtained from a matched model against test data. In order to evaluate the impact of the structural deflections on the conjugate heat transfer, the experimentally measured displacements are applied to the different models and run separately.

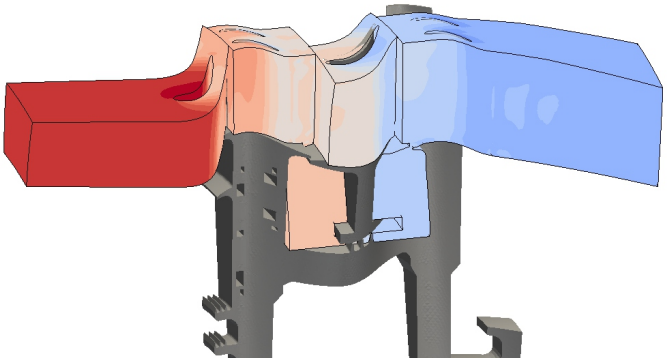

Figure 3. Extent of the 3D CFD sector geometry contoured by total temperature superimposed with the 3D SC03 sector model (grey)

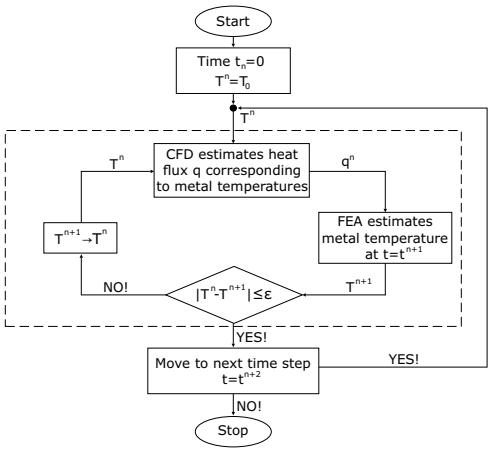

Figure 4. Schematic representation of the aerothermal coupling process

In order to perform the coupled thermal analyses, 3D CFD models are created fitting the extent of the 3D FEA. Therefore, four grids are generated to discretise the two relevant geometries. At first, each case is meshed using the cold running clearances. In a second step, the experimentally measured radial deflections obtained from the experiments are applied to both geometries and then meshed. The extent of the obtained 3D CFD sector model coloured by total temperature can be seen in Fig. 3, as it is superimposed to the FEA model.

The computational domain is meshed using the Rolls-Royce in-house automatic meshing tool PADRAM (Parametric Design and Rapid Meshing).[16] For both designs, the main annulus and the baseline cavity, high fidelity, fully multi-block structured meshes are produced, whereas for the deflector plate cavity hybrid unstructured meshes are generated. Adequate mesh size and topology sensitivity studies were conducted as reported in previous works.[7,17] Grids of around a million cells per vane, plus four million cells in the baseline cavity and five million cells for the deflector plate cavity are created. The connections at the rim between the main annulus and the cavities are achieved in a conformal way. Details on the modelling approaches and the mesh convergence for both geometries can be found in the studies of Dixon et al.[3] and Pohl et al.,[7] respectively.

The commercial code FLUENT is used, for which the RANS equations are solved using second order finite volume discretisation of the domain in double precision. The $k-\omega$ SST turbulence model proposed by Wilcox [18] is used after having been employed successfully in re-ingestion and FEA-CFD coupled studies by Guijarro et al.[19] and Dixon et al.[3] $y^+ < 1$ values are achieved in order to accurately resolve the viscous sublayer and heat transfer. Each case is run in a steady-state condition where the communication between stationary and rotating reference frames is achieved by mixing planes. The convergence of the numerical simulations is primarily assessed by monitoring residuals of mass, energy, and momentum equations and secondarily by checking mass balance (smaller than 0.1 % discrepancy) and enthalpy balance (smaller than 3 % discrepancy) of the converged solution.

The results presented here are based on the thermal coupling between the in-house FEA solver SC03 and the commercially available CFD code FLUENT. Both codes communicate through a Rolls-Royce proprietary library. It is within this functionality that the user specifies one or more coupled walls, outlining a CFD domain, which may cover a part or the whole of the finite element model. A schematic illustration of the process is depicted in Fig. 4, whilst a more detailed description is given by Verdicchio et al. for any CFD code application.[20]

III.B. Optimisation Strategy

The optimisation is conducted using the Rolls-Royce SOPHY system (SOFT, PADRAM, HYDRA).[21] SOFT (Smart Optimisation For Turbomachinery)[22] provides a library of different optimisation algorithms and communicates through python scripts with the other codes in order to execute them in batch mode, to evaluate the results of the simulation. In general, these computations are run in parallel on an HPC cluster in order to reduce the overall run time.

The geometry used in this work is also based on the MAGPI rig test facility as described above. In order to keep the computational requirements within the capability of available computer facilities, it was decided to reduce the size of the discretised domain to a minimum. As in the previous numerical study on the original deflector plate geometry,[7] in this work a 1/39th sector model is chosen, which is a reasonable approximation due to the periodicity of the 78 blades and 39 vanes per stage. Furthermore,

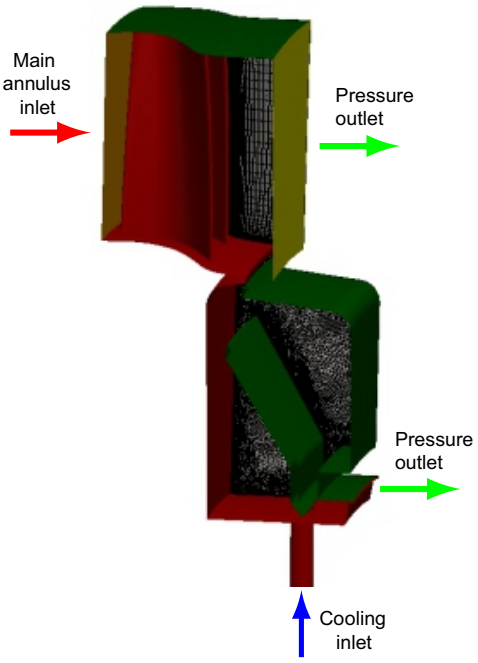

Figure 5. Extent of the 3D CFD sector model used during the design optimisation

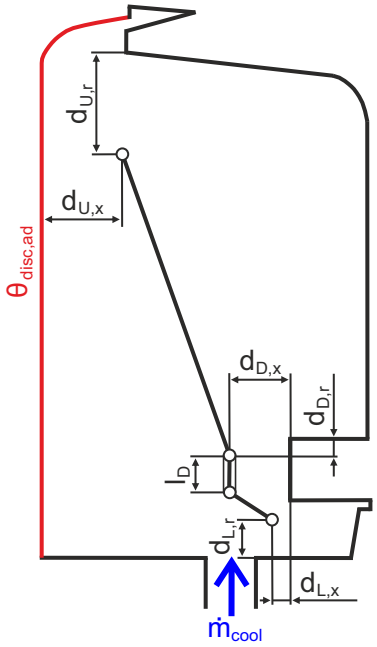

Figure 6. Parametric definition of the deflector plate inside the cavity

the two stage domain is reduced to only one rotor blade pair from the first stage and the upstream cavity including the deflector plate until the first fin of the interstage seal (see Fig. 5).

The mesh is generated as described in the previous section. At this stage the Rolls-Royce in-house CFD code HYDRA is used to solve the RANS equations using a second order finite volume discretisation of the domain in double precision. Following the recommendation of previous computational validation studies,[4,8,10,19] the turbulence closure was done using the $k-\omega$ turbulence model with adaptive wall functions of Launder and Spalding[23] in the regions where the near wall resolution was large.

The cooling air inlet is defined as a mass flow inlet with a fixed temperature. The inlet for the main annulus is defined as a pressure inlet, where the total pressure is read across from the solution of the complete main annulus. The same approximations are taken for the outlets in the main annulus and the fin, where the static pressure distributions are taken from the full sector model run.

The walls are defined as adiabatic, to keep the computation within a reasonable time scale. During the early design phase of the MAGPI test rig, similar stand-alone adiabatic CFD simulations were carried out to get an idea of the impact on the disc temperature using different geometries and varying amounts of cooling air.[17]

The cavity geometry and the rotor geometry are not changed in this study. Only the shape and the position of the deflector plate are modified. The parameterisation of the deflector plate is done in 2D and is shown in Fig. 6. In total seven geometrical design parameters are defined:

- $d_{U,x}$ and $d_{U,r}$, which define the axial and radial degree of freedom of the upper point
- $d_{D,x}$, which defines the axial distance of the vertical bar to the stator foot
- $d_{D,r}$, which defines the radial degree of freedom of the point connecting the upper section to the vertical bar with respect to the outer radii of the stator foot
- l_D, which defines the length of curve vertical bar
- $d_{L,x}$ and $d_{L,r}$, which define the axial and radial degree of freedom of the lower point

In order to finally setup the automated optimisation loop, an objective function as well as the constraints have to be defined, both depicted in Fig. 6 by the blue arrow and the red contour line, respectively. The objective of this optimisation is to minimise the cooling air mass flow rate entering the cavity through the drive arm hole and defined as follows:

$$f(\mathbf{x}) = \dot{m}_{cool} \tag{1}$$

with $\mathbf{x}$ being the design vector consisting of eight design parameters (seven geometrical and one for the cooling air mass flow rate). Also one constraint $g_j(\mathbf{x})$ is defined (see Fig. 6):

$$g_j(\mathbf{x}) = \theta^{max}_{disc,ad} - \theta_{disc,ad,j} \geq 0 \tag{2}$$

where $\theta^{max}_{disc,ad}$ is the non-dimensional maximum allowable area mean adiabatic wall temperature at the disc and $\theta_{disc,ad,j}$ the computed value for a particular design j. The maximum value is taken from the results of a numerical simulation of the baseline geometry without a deflector plate and an initial cooling mass flow rate of 55gs^{-1}, which is set to $100\,\%\,\dot{m}_{cool}$ in this study.

The actual optimisation is based on regressing Kriging and is described in detail in the papers of Pohl et al.[8,9] The computation is conducted in parallel, where each CFD simulation is run on 24 cores.

IV. Results

In this section the results of the two studies are presented and discussed. At first, the impact of structural deflections on the metal temperature predictions is presented, which is followed by the results of the automated design optimisation.

IV.A. Impact of Structural Deflections on Metal Temperature Predictions

At first, the test case for the baseline geometry is evaluated which is followed by the evaluation of the test case with an included deflector plate. Both geometries are run at cold and hot running clearances in order to highlight the structural impact on the TSW heat transfer. The results of the aerothermal coupling for both designs with cold and hot clearances are shown in Figs. 7 and 8. On the left hand side the temperature predictions for the cold geometry are shown, in the middle the metal temperatures for the hot one. As the differences are hard to distinguish from these two separate representations, a difference plot for each flow case is illustrated on the right hand side of the same figure. The difference is taken by subtracting the cold from the hot solution.

Analysing the baseline case first (Fig. 7), it can be seen that the differences in temperature between the cold and hot geometry are locally significantly different. This is in particular the case in the upstream rim region at both the rotor and the stator. These differences propagate along the stator foot to lower radii. The remaining rotor parts are almost at an identical temperature regardless the choice of the seal clearance. This can be explained with local hot gas ingestion into the upstream cavity, which then penetrates the cavity along the stator once the interstage seal opens. As the amount of hot gas ingestion is only minor compared to the amount of coolant, the core flow is marginally affected and so is the rotor disc temperature.

As for the baseline design, the deflector geometry with cold and hot clearances is analysed using the coupled conjugate heat transfer method. The metal temperature contours for both seal clearances (cold on the left and hot in the middle) and the respective difference plot (right hand side) is represented in Fig. 8.

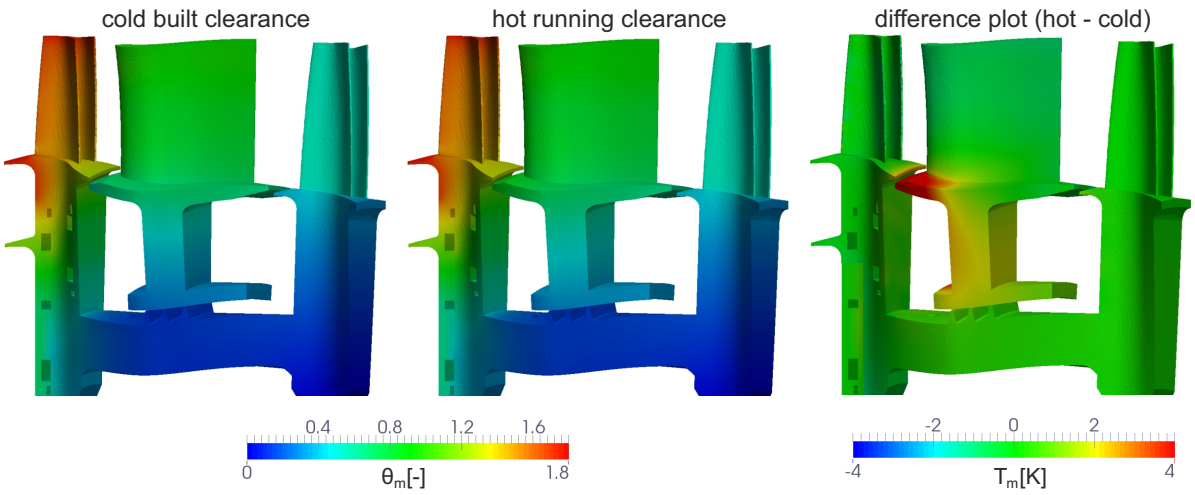

Figure 7. Metal temperature contours of the baseline design for the cold (left) and hot geometries (middle) including the respective temperature difference contours (right)

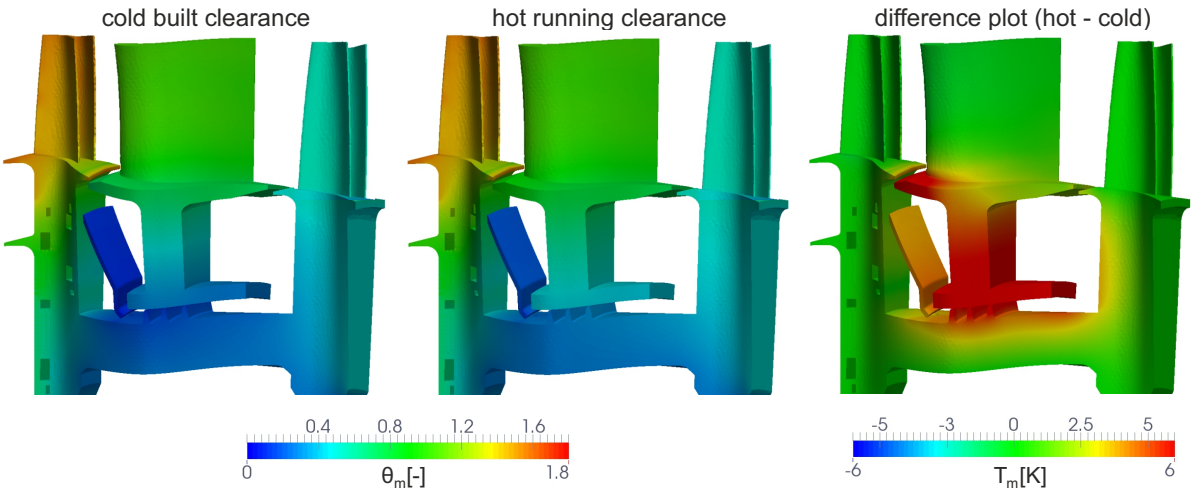

Figure 8. Metal temperature contours of the deflector plate design for the cold (left) and hot geometries (middle) including the respective temperature difference contours (right)

Compared to the baseline simulation, the impact of taking into account the structural deformations on the metal temperature predictions is more significant. The rim as well as the stator foot are significantly hotter when using the hot running clearance. Furthermore, the rotor rim is hotter as well as the interstage seal fins. However, the uptream rotor disc is only marginally affected. Again, these higher temperatures can be associated to the local hot gas ingestion, which is present when opening the interstage seal.

Both comparisons of these results against experimental test data showed that the predictions matched the experiments better[10] due to the shift to higher values, which is related to the hot gas ingestion. This is particularly true along the stator. Slight improvements are also achieved at the rotor disc. However, the discrepancies at the rotor rim are still in an unacceptable range. An explanation for this mismatch is the lack of accuracy of steady-state CFD to predict the turbulent mixing in the rim region. Therefore, in future it is recommended to use unsteady CFD or higher order turbulence models such as LES rather than steady-state CFD in order to correctly predict the rotor rim temperatures.

IV.B. Optimisation Results

In this section, first steady-state adiabatic CFD analyses are carried out in order to evaluate the optimised TSW flow field with a reduced amount of cooling air and then the outcome of the optimisation is validated. Furthermore, this new flow field is compared against the flow field of the non-optimised design with the same amount of coolant. By doing this, the main advantages of the new design are highlighted.

In a second part, a back-to-back comparison of the metal temperatures of the optimised and non-optimised design with a reduced amount of cooling air is carried out. This is done to gain more confidence in the current optimisation methodology, where stand-alone CFD simulations are used to improve the metal component cooling. Furthermore, the comparison highlights the main differences between the optimised and non-optimised deflector design at a reduced coolant flow rate.

A comparison of the flow fields of the optimised deflector plate design (top) against the non-optimised (bottom) with respect to the position and shape based on the findings from the optimisation[8,9] can be seen in Fig. 9: the upper tip of the deflector is moved close to the rotor disc, whereas the lower parts are moved close to the stator foot. The depicted mid-plane cuts are surface LIC (i.e. line integrated convolution) representations contoured by swirl fraction β ($= v_{theta}/(\omega r)^{-1}$). Both simulations are run with a reduced cooling mass flow rate of $0.35\,\dot{m}_{cool}$.

For the optimised deflector plate geometry, it can be seen that the cooling air enters the cavity swirled at disc speed ($\beta = 1$) and keeps its swirl as long as it does not impinge the deflector plate. This maintenance of swirl due to the position of the deflector close to the stator foot is beneficial for the cooling performance of the disc. Considering the non-optimised deflector, the cooling air loses all its swirl quickly after entering the cavity even before impinging the deflector.

Another interesting phenomenon can be seen at the lower tip of the deflector plate, where - for the optimised design - part of the highly swirled cooling air seems to move to the interstage seal straight away without cooling the disc. This ensures that the gap between the deflector lower tip and the rotor wall is sealed against hot gas coming from higher radii. This is not the case for the non-optimised geometry.

A comparison of mass flow rates passing the gap between the upper deflector plate tip and the rotor

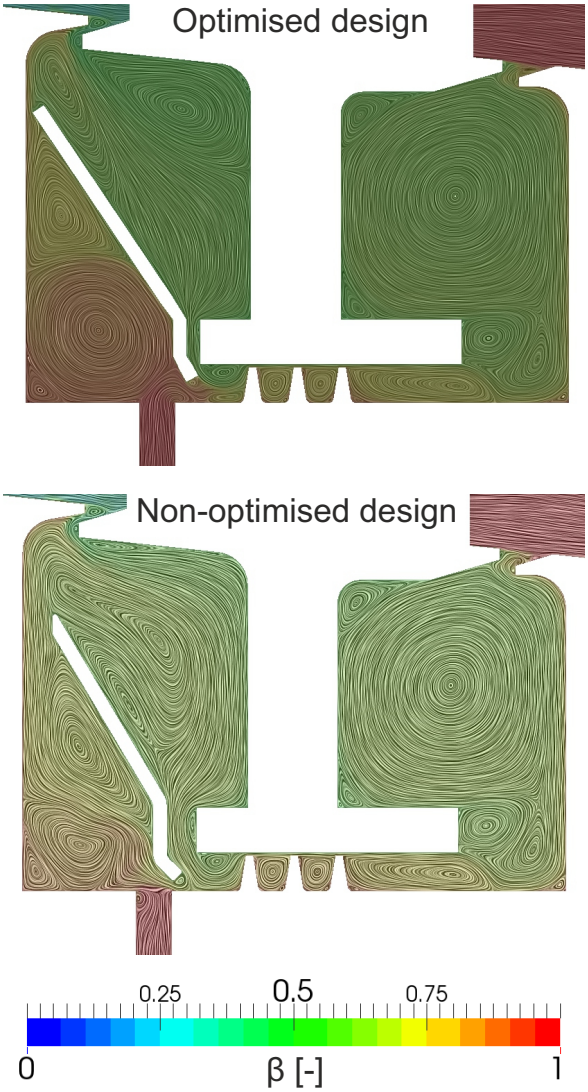

Figure 9. Surface LIC representation contoured by swirl fraction for the optimised (top) and non-optimised (bottom) deflector plate design with the minimised cooling mass flow rate

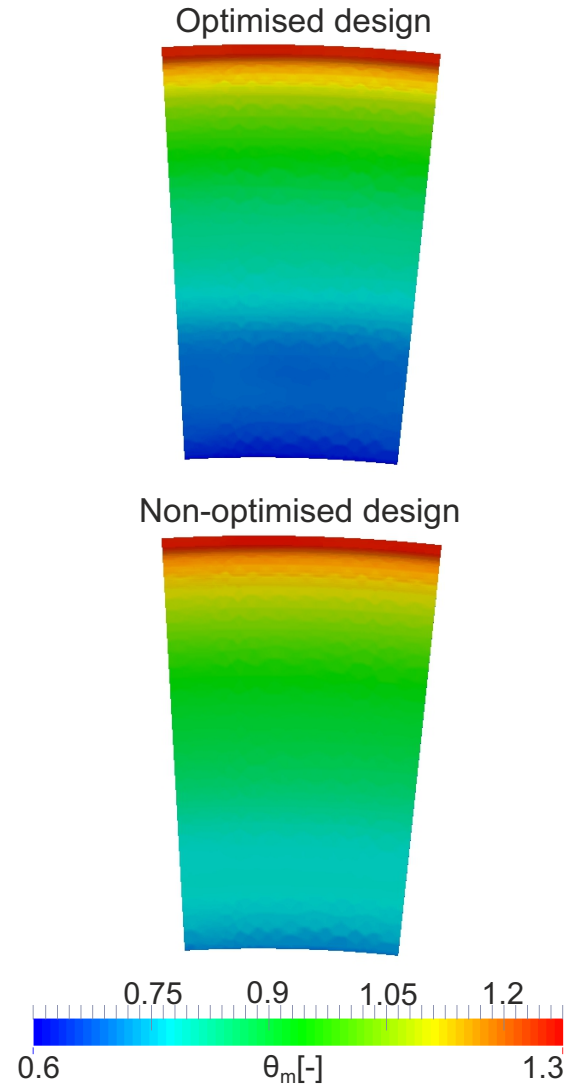

Figure 10. Comparison of the non-dimensional metal temperatures at the upstream rotor disc for the optimised (top) and non-optimised (bottom) deflector plate design with the minimised cooling mass flow rate

disc shows a significant difference in the two designs and supports the previous assumptions: for the optimised deflector plate a mass flow rate of around $0.28\,\dot{m}_{cool}$ passes the gap whereas for the non-optimised design the mass flow rate is $0.76\,\dot{m}_{cool}$. This indicates that, for the optimised design, a portion of cooling air is used to seal the gap at the lower tip from hot gas recirculation and in the non-optimised design a significant amount of hot gas is recirculated instead. This should also reflect in the rotor disc temperatures.

In Fig. 10, the rotor disc metal temperature contours obtained from the aerothermal coupling for both cases are depicted. On the top the contours for the optimised deflector plate design are depicted and on the bottom for the non-optimised design, both at a reduced coolant mass flow rate. From these two plots it can be seen that the optimised deflector design provides a better disc cooling, which one could already infer from the swirl contours.

Having said that, it can be concluded that the optimisation converged to a better deflector design, keeping the rotor disc cool while reducing the amount of cooling air. However, a large amount of hot gas enters the cavity, which inevitably results in a heatup of the metal of the stationary components. Also it is worth mentioning that the simulations are run with a constant interstage seal clearance only. The thermo-mechanical impact of the stator heating on the interstage seal clearance is not considered although this would need to be taken into consideration in any real engine design (as covered in the previous section).

V. Conclusion

In this paper two separate studies are presented. At first the impact of structural deflections on the heat transfer in TSWs is analysed using cold and hot interstage seal clearances, which were obtained from experiments. A fully automated FEA-CFD coupling capability was demonstrated and results from two different models were compared.

It was found that the use of hot running clearances results in an increase of stator metal temperatures inside the TSW, which are in better agreement with the experimental measurements. However, the discrepancies in the rotor rim region still persist in the predictions. It will be desirable to incorporate unsteadiness and higher order turbulence models in the CFD solution. Findings in previous works[7,19] showed how the flow unsteadiness caused by the rotor-stator interaction modifies the rotor downstream wakes and therefore the turbulence mixing near the rim gap.

In the second part, an automated design optimisation using Kriging of a 3D sector model of a TSW test rig geometry with an inserted stationary deflector plate has been carried out. The geometry has been parameterised in such a way that flexibility of the design is ensured: different shapes and positions of the deflector plate inside the cavity have been generated automatically.

The outcome of the optimisation using adiabatic steady-state CFD has shown that the optimised design provides better rotor disc cooling than the non-optimised design. This outcome has been verified using the coupled FEA-CFD method to compare metal temperatures for the new design to those for the non-optimised design. These results were in agreement with the stand-alone CFD results.

For future work in this research area, some recommendations are given here. When applying this method to real engine running conditions, the thermo-mechanical movements are very important. Not only, is it likely that a variation in seal size affects the final flow solution, but also the very extreme positions of the deflector should be chosen very carefully in order to prevent rubbing and damage at the most critical running conditions.

Acknowledgements

The present investigations were supported by the European Commission within the AMEDEO Marie Curie initial training network (grant reference 316394) and the authors want also to thank the European Commission for its support within the Framework 6 Programme, Research Project MAGPI, AST5-CT-2006-030874 for the use of the test rig geometry.

A special mention must be made to Rolls-Royce staff Christopher Barnes, Shahrokh Shahpar and Ralf Schlaps for their support as well as Jeff Dixon for his technical advice.

References

[1]AMEDEO, 2013. Aerospace Multidisciplinary Enabling Design Optimisation. Grant reference: 316394.

[2]MAGPI, 2006. Main Annulus Gas Path Interaction - Specific Targeted Research Project. Proposal Contract no.: 30874.

[3]Dixon, J. A., Guijarro-Valencia, A., Coren, D., Eastwood, D., and Long, C., 2014. "Main Annulus Gas Path Interactions - Turbine Stator Well Heat Transfer". *J Turbomach,* **136**, February, pp. 021010–1–16.

[4]Smith, P. E. J., Mugglestone, J., Tham, K. M., Coren, D. D., and Long, C. A. "Conjugate Heat Transfer CFD Analysis in Turbine Disc Cavities". *ASME Turbo Expo GT2012-69597.*

[5]Andreini, A., DaSoghe, R., and Facchini, B., 2011. "Turbine Stator Well CFD Studies: Effects of Coolant Supply Geometry on Cavity Sealing Performance". *J Turbomach,* **133**, April, pp. 021008–1–11.

[6]Lück, H., Schäfer, M., and Schiffer, H.-P. "Simulation of Thermal Fluid-Structure Interactions in Blade-Disc Configuration of an Aircraft Turbine Model". *ASME Turbo Expo GT2014-26316.*

[7]Pohl, J., Fico, V., and Dixon, J. A., 2015. "Turbine Stator Well Cooling - Improved Geometry Benefits". In ASME Turbo Expo 2015, GT2015-42658.

[8]Pohl, J., Thompson, H. M., Guijarro Valencia, A., López Juste, G., Fico, V., and Clayton, G. A. "Structural Deflection's Impact in Turbine Stator Well Heat Transfer". *to appear in J Eng Gas Turb Pow.*

[9]Pohl, J., Thompson, H. M., Schlaps, R. C., Shahpar, S., Fico, V., and Clayton, G. A., 2016. "Innovative Turbine Stator Well Design Using Design Optimisation". In 16th ISROMAC & 1st ISIMET.

[10]Pohl, J., Thompson, H. M., Schlaps, R. C., Shahpar, S., Fico, V., and Clayton, G. A. "Innovative Turbine Stator Well Design Using a Kriging Assisted Optimisation Method". *to appear in J Eng Gas Turb Pow.*

[11]Daily, J. W., and Nece, R. E., 1960. "Chamber Dimension Effects on Induced Flow and Frictional Resistance of Enclosed Rotating Disks". *J Basic Eng-T ASME,* **82**, pp. 217–232.

[12]Phadke, U. P., and Owen, J. M., 1988. "Aerodynamic Aspects of the Sealing of Gas Turbine Rotor-Stator Systems - Part 1: The Behaviour of Simple Shrouded Rotating Disk Systems in Quiescent Environment". *Int J Heat Fluid Flow,* **9**, pp. 98–105.

[13]Phadke, U. P., and Owen, J. M., 1988. "Aerodynamic Aspects of the Sealing of Gas Turbine Rotor-Stator Systems - Part 2: The Behaviour of Simple Seals in Quasi-Axisymmetric External Flow". *Int J Heat Fluid Flow*, **9**, pp. 106–112.

[14]Eastwood, D., Coren, D. D., Long, C. A., Atkins, N. R., Childs, P. R. N., Scanlon, T. J., and Guijarro-Valencia, A., 2012. "Experimental Investigation of Turbine Stator Well Rim Seal, re-Ingestion and Interstage Seal Flows Using Gas Concentration Techniques and Displacement Measurements". *J Turbomach,* **134**, August, pp. 082501–1–9.

[15]Eastwood, D., 2014. "Investigaton of Rim Seal Exchange and Coolant Re-Ingestion in Rotor Stator Cavities Using Concentration Techniques". PhD thesis, University of Sussex, Sussex, UK.
[16]Shahpar, S., and Lapworth, L., 2003. "PADRAM: Parametric Design and Rapid Meshing System for Turbomachinery Optimisation". *Power-Gen International,* **6**, pp. 579–590.
[17]Dixon, J. A., Guijarro-Valencia, A., Bauknecht, A., Coren, D., and Atkins, N., 2013. "Heat Transfer in Turbine Hub Cavities Adjacent to the Main Gas Path". *J Turbomach,* **135**, March, pp. 021025–1–14.
[18]Wilcox, D. C., 1998. *Turbulence Modeling for CFD*. DCW Industries.
[19]Guijarro-Valencia, A., Dixon, J. A., Soghe, R. D., Facchini, B., Smith, P. E. J., Muñoz, J., Eastwood, D., Long, C. A., Coren, D., and Atkins, N. R. "An Investigation Into Numerical Analysis Alternatives For Prediciting Re-Ingestion in Turbine Disc Rim Cavities". *ASME Turbo Expo GT2012-68592*.
[20]Verdicchio, J. A., 2001. "The Validation and Coupling of Computational Fluid Dynamics and Finite Element Codes for Solving Industrial Problems". PhD Thesis, University of Sussex, Sussex, UK, July.
[21]Shahpar, S., 2005. SOPHY: An Integrated CFD Based Automatic Design Optimisation System. Report No. ISABE-2005-1086.
[22]Shahpar, S., 2002. "SOFT: A New Design And Optimisation Tool for Turbomachinery". In CIMNE 2002, K. G. et al., ed.
[23]Launder, B. E., and Spalding, D. B., 1974. "The Numerical Computation of Flows". *J Comp Meth Appl Mech Eng,* **3**, pp. 269–289.